

Tetrahedral vs. polyhedral mesh size evaluation on flow velocity and wall shear stress for cerebral hemodynamic simulation

Martin Spiegel^{a,b,c,d,*}, Thomas Redel^c, Y. Jonathan Zhang^e, Tobias Struffert^b, Joachim Hornegger^{a,d}, Robert G. Grossman^c, Arnd Doerfler^b and Christof Karmonik^c

^aPattern Recognition Lab, Department of Computer Science, Friedrich-Alexander University Erlangen-Nuremberg (FAU), Erlangen, Germany; ^bDepartment of Neuroradiology, FAU, Erlangen, Germany; ^cSiemens AG Healthcare Sector, Forchheim, Germany; ^dErlangen Graduate School in Advanced Optical Technologies (SAOT), Erlangen, Germany; ^eThe Methodist Hospital Research Institute, Houston, TX, USA

(Received 11 May 2010; final version received 23 August 2010)

Haemodynamic factors, in particular wall shear stresses (WSSs) may have significant impact on growth and rupture of cerebral aneurysms. Without a means to measure WSS reliably *in vivo*, computational fluid dynamic (CFD) simulations are frequently employed to visualise and quantify blood flow from patient-specific computational models. With increasing interest in integrating these CFD simulations into pretreatment planning, a better understanding of the validity of the calculations in respect to computation parameters such as volume element type, mesh size and mesh composition is needed. In this study, CFD results for the two most common aneurysm types (saccular and terminal) are compared for polyhedral- vs. tetrahedral-based meshes and discussed regarding future clinical applications. For this purpose, a set of models were constructed for each aneurysm with spatially varying surface and volume mesh configurations (mesh size range: 5119–258,481 volume elements). WSS distribution on the model wall and point-based velocity measurements were compared for each configuration model. Our results indicate a benefit of polyhedral meshes in respect to convergence speed and more homogeneous WSS patterns. Computational variations of WSS values and blood velocities are between 0.84 and 6.3% from the most simple mesh (tetrahedral elements only) and the most advanced mesh design investigated (polyhedral mesh with boundary layer).

Keywords: mesh size evaluation; mesh independence analysis; polyhedral; tetrahedral; wall shear stress; blood flow velocity

1. Introduction

Ischaemic stroke, being the third common cause of death in the western world, is a serious clinical event. Of the two main causes of a stroke, arterial obstruction and intra-cerebral haemorrhage, about 10–15% of the latter are induced by the rupture of a cerebral aneurysm (Winn et al. 2002). More and more cerebral aneurysms are now incidentally detected because of recent advances in the field of medical imaging techniques such as 64 slice computed tomography (CT) or magnetic resonance imaging (MRI) at 3T. So far, the reason for growth or rupture of an aneurysm is not entirely understood, but it is assumed that the haemodynamic within an aneurysm plays an important role (Jou et al. 2008). Geometric factors, e.g. lesion size and aspect ratio (AR) (Ujiie et al. 2001; Nader-Sepahi et al. 2004; Raghavan et al. 2005) are also considered to determine the risk of rupture. However, even haemodynamic information together with geometric aspects has so far proven insufficient for the calculations of a reliable patient-specific risk index for a particular aneurysm. Other biological mechanisms and systemic conditions may also contribute to aneurysm

rupture. To assess intra-aneurysmal haemodynamics, computational fluid dynamic (CFD) simulations have been employed with patient-specific geometries derived from clinical image data in Steinman et al. (2003), Hoi et al. (2004), Karmonik et al. (2004), Shojima et al. (2004), Cebal and Lohner (2005), Cebal et al. (2005b) and Venugopal et al. (2007). A reliable patient-specific CFD-based blood flow simulation will be strongly influenced by two factors: (1) the geometric accuracy of the patient-specific vascular model dependent on the segmentation method used and (2) the boundary conditions and simulation parameters such as inflow blood speed, blood density/viscosity and rigid walls. Patient-specific boundary conditions can either be obtained through invasive measurements during treatment (i.e. pressure catheter) or, as demonstrated recently, by 2-D phase-contrast MRI providing the time-varying blood flow profile at the inlet of the computational model as shown in Karmonik et al. (2008). The sensitivity of other computational parameters on the simulation results, in particular mesh size and mesh design, has not been evaluated in detail for this particular vascular pathology. The haemodynamic situation in cerebral aneurysms is favourable to be simulated

*Corresponding author. Email: martin.spiegel@informatik.uni-erlangen.de

using CFD: blood flow in cerebral vessels is always antegrade as compared to the blood flow in the aorta with modest pulsatility. Unless downstream vascular disease is present such as a stenotic lesion distal to the aneurysm, vascular resistance is low. Reynolds numbers are low (in the order of 100 s) and, therefore, no turbulence flow can be expected. Due to these favourable conditions, most studies so far have successfully employed simple meshes such as tetrahedral meshes with no adaptation or boundary layer. Still, the assessment of the mesh quality is considered as a very important task, because inaccurate meshing including high skewness (SN) of cells or course spatial resolution may lead to non-valid CFD results and thus leading to potentially inaccurate local velocities or wall shear stress (WSS) patterns. In particular, for a future clinical CFD-based diagnostic and treatment tool, the performed simulations have to be fast and stable. The mesh size has to be as small as possible, but concerning accuracy as fine as necessary to avoid numerical prediction errors (velocity and WSS). Two different approaches are known to verify the mesh suitability for CFD simulation introduced by Prakash and Ethier (2001): (1) Comparison of CFD results with experimental measured data and (2) a mesh independence analysis. This work applies the second approach to evaluate the impact of varying surface and volume mesh resolutions as well as different meshing techniques represented by polyhedral (Oaks and Paoletti 2000) and tetrahedral meshes. In particular, the question which mesh granularity can be considered as accurate enough to get reliable blood flow simulation results is investigated with time restraints existing for future clinical applications in mind. A preliminary version of this work was reported by Spiegel et al. (2009). Two cerebral vessel geometries were investigated, i.e. a sidewall aneurysm of the internal carotid artery and a basilar bifurcation aneurysm as depicted in Figure 1. Blood flow velocity and WSS distributions according to varying spatial mesh resolutions and configurations (polyhedral vs. tetrahedral elements) are evaluated. Effects of boundary layer regarding WSS are studied by means of comparing boundary layer-based meshes with those exhibiting no boundary layer. Unsteady simulations are performed with varying time step (TS) to determine the largest step delivering still valid simulation results.

2. Methods

3-D digital subtraction angiography image data (Heran et al. 2006) of the two cerebral aneurysms (see Figure 1) were acquired during endovascular interventions using Siemens C-arm System (AXIOM Artis dBA, Siemens AG Healthcare Sector) in Forchheim (Germany) and Houston, TX (USA). 3-D image reconstructions of both aneurysms led to an image volume for case 1 of $138.24 \times 138.24 \times 57.72$ mm with a voxel spacing of $0.27 \times 0.27 \times 0.13$ mm and for case 2 $97.28 \times 97.26 \times 66.43$ mm (voxel spacing $0.19 \times$

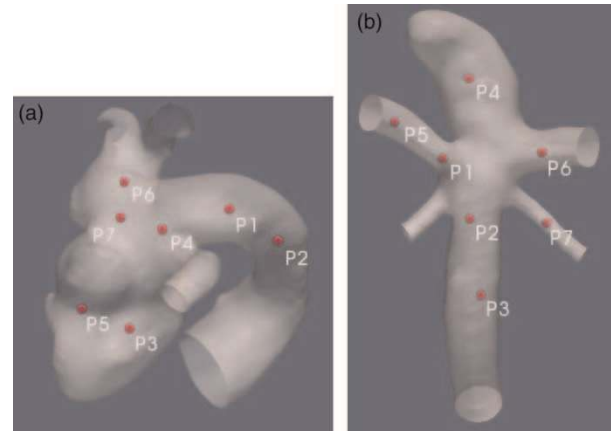


Figure 1. 3-D mesh representations of the evaluated aneurysms: (a) case 1 depicts an internal carotid aneurysm and (b) case 2 illustrates a basilar tip aneurysm. The red spheres show the positions of the velocity measurement points distributed in the vicinity of the aneurysms, i.e. at the inlet, within the aneurysm and at the outlet.

0.19×0.1 mm), respectively. The non-isotropic voxel spacing comes from image downsampling in x/y -direction due to segmentation and memory issues. For mesh generation and smoothing, the marching cubes (Lorenson and Cline 1987) and a Laplacian-based smoothing algorithm (VTK Kitware Inc., Clifton Park, NY, USA) were applied as an additional step. The image data were stored as a stereolithographic file providing the input data for the meshing software GAMBIT (ANSYS Inc., Canonsburg, PA, USA). The mesh corresponding to case 1 exhibits a volume of 537 mm^3 and the mesh of case 2 of 282 mm^3 . The maximal diameters of the inlet and outlets are as follows: (1) case 1: inlet 5.2 mm, outlet 1 2.0 mm, outlet 2 2.3 mm and outlet 3 2.6 mm and (2) case 2: inlet 3.3 mm, outlet 1 2.5 mm, outlet 2 1.5 mm, outlet 3 1.5 mm and outlet 4 2.4 mm.

Different surface mesh resolutions were generated by using the GAMBIT curvature size function (Cooperation 2007). This function constrains the angle between outward-pointing normals for any two adjacent surface triangles. That leads to a denser mesh resolution in areas exhibiting high curvature like the aneurysm and coarser resolution in more flat regions. Four parameters define the curvature size function, i.e. angle, growth, max. and min. triangle size. Table 1 contains a detailed overview of the applied curvature size function parameters as well as the set of meshes. The final number of triangles representing the surface mesh is automatically determined by the meshing algorithm according to the chosen parameter values and the geometry. The resolution of the surface mesh rules the final number of tetrahedral control volume elements – the larger the number of surface triangles, the larger is the number of tetrahedral control volume elements.

To study the effects of boundary layer usage, almost all meshes (see Table 1) were generated without and with

Table 1. Set of meshes – case 1 and case 2.

	#Tet. cells (BL)	Difference no-BL to BL for Tet. cells in (%)	#Poly. cells (BL)	Difference no-BL to BL for Poly. cells in (%)	Difference Poly. vs. Tet. in (%)	Difference Poly. vs. Tet. BL in (%)	Difference BL vs. Tet. non-BL in (%)	Max./min. triangle	Growth	Angle
Case 1	13,841 (-)	-	5119 (-)	-	-	-	-	6/0.001	1.2	25
	26,702 (40,699)	52.4	7288 (24,206)	232.4	-72.7	-40.5	-9.3	3.6/0.001	1.2	14
	52,374 (77,252)	47.5	12,467 (1,548)	153.1	-76.2	-59.2	-39.8	1.8/0.001	1.1	14
	76,493 (109,638)	43.3	17,695 (38,564)	117.9	-76.9	-64.8	-49.6	1.2/0.001	1.2	6
	86,621 (107,336)	23.9	18,681 (32,042)	71.4	-78.4	-70.2	-63.0	0.4/0.001	1.1	12
	106,010 (124,041)	17.0	22,297 (35,866)	60.9	-79.0	-71.1	-66.2	0.36/0.001	1.1	12
	115,014 (160,771)	39.8	25,540 (48,687)	90.6	-77.8	-69.7	-57.7	0.3/0.001	1.1	10
	189,625 (202,565)	6.8	37,495 (53,794)	43.5	-80.2	-73.4	-71.6	0.28/0.001	1.1	10
	197,098 (228,097)	15.7	38,991 (58,879)	51.0	-80.2	-74.2	-70.1	0.27/0.001	1.1	10
	231,354 (258,481)	11.7	45,158 (65,707)	45.5	-80.5	-74.6	-71.6	0.258/0.001	1.1	10
Case 2	31,696 (47,311)	49.3	8814 (26,014)	195.1	-72.2	-45.0	-17.9	0.42/0.001	1.2	17
	43,063 (59,914)	39.1	10,843 (21,153)	95.1	-74.8	-64.7	-50.9	0.37/0.001	1.17	17
	56,176 (75,447)	34.3	13,280 (24,978)	88.1	-76.4	-66.9	-55.5	0.34/0.001	1.12	15
	75,469 (100,587)	33.3	16,795 (30,435)	81.2	-77.4	-69.7	-59.7	0.32/0.001	1.10	13
	98,399 (129,516)	31.6	21,108 (37,221)	76.3	-78.6	-71.3	-62.2	0.3/0.001	1.10	10
	114,227 (142,336)	24.6	23,846 (39,833)	67.0	-79.1	-72.0	-65.1	0.28/0.001	1.10	10
	148,625 (159,797)	7.5	30,167 (44,652)	48.0	-79.7	-72.1	-70.0	0.25/0.001	1.09	8
	184,226 (219,922)	19.4	36,845 (65,398)	77.5	-80.0	-70.3	-64.5	0.24/0.001	1.10	6
Avg.		29.2		93.8	-77.7	-66.5	-55.6			

Tet. and Poly., tetrahedral and polyhedral, respectively and BL., boundary layer.

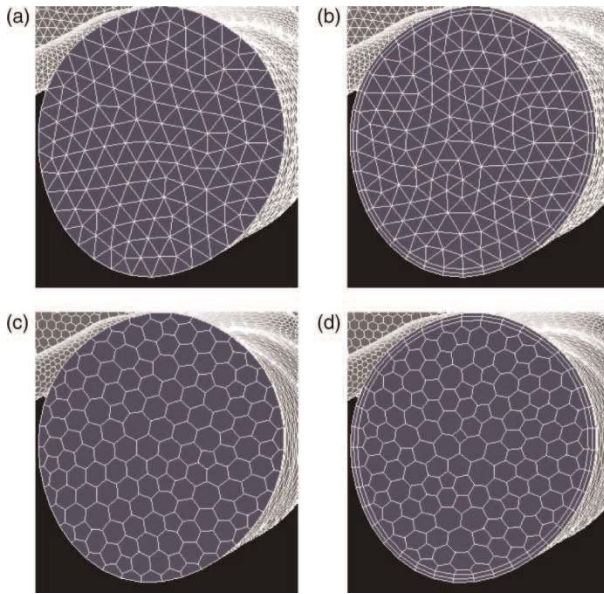


Figure 2. Meshing example regarding case 2. (a) and (c) show tetrahedral and polyhedral meshes. (b) and (d) depict tetrahedral and polyhedral-based meshes with a boundary layer.

boundary layers (Garimella and Shephard 2000; Loehner and Cebal 2000). Since a boundary layer approximates the boundary of the vessel tubes with prisms as shown in Figure 2, this automatically results in a higher number of tetrahedral control elements as compared to meshes without a boundary layer. The boundary layers were created through GAMBIT's boundary layer algorithm featuring two levels. The height of the first level was chosen to be 0.04 mm and the second one 20% larger, i.e. 0.048 mm. The mesh quality in terms of AR and surface/mesh SN is summarised in Table 2.

The tetrahedral meshes were imported into the simulation software Fluent (ANSYS Inc.). A conversion algorithm, part of the Fluent CFD solver, was used to generate for each tetrahedral mesh a corresponding polyhedral mesh. The surface of the vessel models was assumed to be rigid walls and no slip as shear condition. Blood was modelled as an incompressible Newtonian fluid with a density of 1050 kg/m^3 and a viscosity of 0.004 N/m^2 (Hassan et al. 2004). The boundary conditions for all conducted simulations were as follows: the inlet was considered as velocity inlet and all outlets were modelled as pressure outlet zero. A constant inflow rate of 0.3 and 0.5 m/s was applied in the steady simulations for the case 1 and case 2, respectively. In unsteady simulations, two different inflow waveforms were used (Figure 3): for case 1, an MRI-measured waveform and for case 2, we applied a waveform taken from a former publication (Grodén et al. 2001) which was measured with ultrasound, since there was no patient-specific blood flow profile measured with MRI or ultrasound. Similar blood flow velocity profiles concerning the basilar artery were also measured by Kato et al. (2002). Steady-state simulations were considered as converged if the relative residuals fall under 0.001 (i.e. the absolute values of the residuals were reduced by 3 orders of magnitude). In addition, the mass flow was measured to prove convergence by subtracting outflow from inflow. All converged solutions exhibit a mass flow difference between inflow and outflow of $\pm 5 e^{-8}$.

Seven points were defined to measure the simulated blood flow velocity occurring in the environment of the aneurysm. In case 1, two points were placed in the inlet region of the aneurysm, three inside the aneurysm dome and two in the outlet region of the aneurysm. In case 2, one point was located within the inlet vessel part, another one

Table 2. Overview mesh quality, i.e. aspect ratio (AR) and skewness (SN) for surface and mesh.

	#Tet. cells (BL)	#Poly. cells (BL)	Surface		Mesh	
			AR	SN	AR	SN
Case 1	26,702 (40,699)	7283 (24,206)	1–1.76	0–0.43	1–4	0–0.75
	52,374 (77,252)	12,467 (31,548)	1–1.52	0–0.40	1–3.19	0–0.77
	76,493 (109,638)	17,695 (38,564)	1–1.60	0–0.48	1–3.34	0–0.80
	86,621 (107,336)	18,681 (32,012)	1–1.74	0–0.51	1–3.52	0–0.77
	106,010 (124,041)	22,297 (35,866)	1–1.63	0–0.46	1–3.28	0–0.78
	115,014 (160,771)	25,540 (48,687)	1–1.53	0–0.45	1–3.34	0–0.74
	189,625 (202,565)	37,495 (53,794)	1–1.62	0–0.49	1–3.31	0–0.77
	197,098 (228,097)	38,991 (58,879)	1–1.55	0–0.46	1–3.28	0–0.77
	231,354 (258,481)	45,158 (65,707)	1–1.44	0–0.40	1–3.43	0–0.75
Case 2	31,696 (47,311)	8814 (26,014)	1–1.62	0–0.49	1–3.10	0–0.76
	43,063 (59,914)	10,843 (21,153)	1–1.62	0–0.49	1–3.22	0–0.76
	56,176 (75,447)	13,280 (24,978)	1–1.41	0–0.38	1–3.10	0–0.78
	75,469 (100,587)	16,795 (30,435)	1–1.42	0–0.38	1–3.31	0–0.76
	98,399 (129,516)	21,108 (37,221)	1–1.63	0–0.50	1–3.19	0–0.77
	114,227 (142,336)	23,846 (39,833)	1–1.38	0–0.36	1–3.25	0–0.76
	148,625 (159,797)	30,167 (44,652)	1–1.58	0–0.47	1–3.34	0–0.75
	184,226 (219,922)	36,845 (65,398)	1–1.56	0–0.46	1–3.31	0–0.77

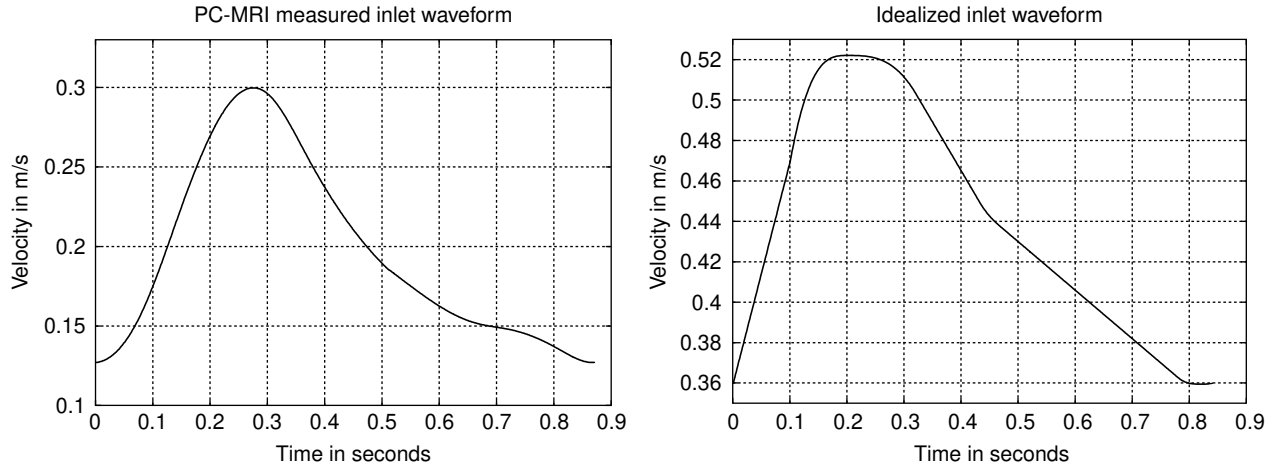


Figure 3. Inlet velocity waveforms applied for unsteady simulations. Left: phase contrast MRI measured blood flow waveform used for case 1. Right: idealised waveform used for case 2. This waveform is inspired by Groden et al. (2001).

inside the aneurysm dome and the remaining points were distributed near the aneurysm neck and within the outlets, respectively. The different point distributions between case 1 and case 2 are reflected in the different vessel geometries, i.e. side wall vs. tip aneurysm. Figure 1 gives a good overview about distributions of the measurement points for both cases. In reality, the points are located inside the geometry.

The simulation experiments performed in this article can be separated into three types as follows:

- (1) Starting with the given number of tetrahedral cells, we compare this number with the corresponding number of polyhedral cells and also without and with boundary layer.
- (2) A series of steady-state simulations is performed to compare tetrahedral vs. polyhedral meshes in terms of velocity and WSS. This series is supposed to shed light on the question what spatial resolution is required to avoid inaccurate CFD results caused by unsuitable CFD meshes. The results were analysed in terms of (A) computational convergence, (B) velocity convergence and (C) WSS convergence. Also, these steady-state simulations were repeated with boundary layer-based meshes to evaluate both the effects on the WSS distribution and the increased complexity concerning the mesh generation process.
- (3) A series of unsteady simulations is conducted according to varying TS, i.e. 1, 5 and 10 ms. The unsteady simulations for both cases were only performed with the highest resolved boundary layer-based polyhedral meshes (see, Table 3 rows 12 and 23). A total of three cardiac cycles were computed and only the results of the second and third cardiac cycle are stored to avoid transient effects as good as possible.

The area-weighted-average WSS distribution was used to express and compare WSS distributions between meshes in terms of numbers. It is defined as follows:

$$\frac{1}{A} \int \phi dA = \frac{1}{A} \sum_{i=1}^n \phi_i |A_i|, \quad (1)$$

where A denotes the total area being considered and ϕ_i describes the WSS associated with the facet area A_i . For the analysis, the complete aneurysmal surface was included but without considering the surrounding vessel segments.

Since tetrahedral-based meshes are considered as state-of-the-art within the simulation community, they are taken as the golden base. Thus, the differences in Tables 3 and 4 between polyhedral and tetrahedral meshes, i.e. number of volume elements (NVE), WSS and iterations are computed by the following formula:

$$\text{diff}_i = \frac{x_i \times 100}{y_i} - 100, \quad (2)$$

$$\text{with } i \in \{\text{\#iter.}, \text{area-weightedaverage WSS}\}, \quad (3)$$

where x_i and y_i denote values given from polyhedral and tetrahedral meshes, respectively.

3. Results

3.1 Cell numbers

Considering Table 1 last row, a boundary layer increased the NVE for tetrahedrals about 29% (column 3) and for polyhedrals about 93% (column 5) on average. Polyhedrals reduced the NVE compared to tetrahedrals about 77% (column 6) on average. Polyhedral meshes with boundary layer needed 66% (column 7) less NVE

Table 3. Summary of the results.

	No boundary layer						
	#Tet. (Poly.) cells	#Iter. Tet. (Poly.)	Difference #Iter. Tet. vs. Poly. in (%)	WSS Tet.	WSS Poly.	Difference WSS Tet. vs. Poly. in (%)	
Case 1	13,841 (5119)	129 (98)	-55.0	4.60	4.66	1.3	
	26,702 (7283)	169 (72)	-57.4	5.39	5.31	1.5	
	52,374 (12,467)	238 (98)	-58.8	5.98	5.73	-4.2	
	76,493 (17,695)	225 (102)	-54.7	6.33	5.94	-6.2	
	86,621 (18,681)	384 (134)	-65.1	6.39	6.03	-5.6	
	106,010 (22,297)	377 (151)	-60.0	6.51	6.07	-6.8	
	115,014 (25,540)	297 (131)	-55.9	6.33	6.08	-4.0	
	189,625 (37,495)	987 (213)	78.4	6.82	6.59	-3.4	
	197,098 (38,991)	815 (214)	-73.7	6.89	6.59	-4.4	
	231,354 (45,158)	1142 (248)	-78.3	7.01	6.69	-4.6	
Average value			63.7	6.76	6.49		
Standard deviation				0.22	0.20		
Uncertainty				3.20%	3.14%		
Case 2	31,696 (8814)	242 (111)	-54.1	5.91	5.26	12.4	
	43,063 (10,843)	378 (176)	-53.7	7.18	6.20	-13.7	
	56,176 (13,280)	365 (185)	-49.3	7.06	6.51	-7.8	
	75,469 (16,795)	437 (202)	-53.8	7.33	6.84	7.3	
	98,399 (21,108)	462 (211)	-54.3	7.43	7.15	-3.7	
	114,227 (23,846)	496 (230)	-53.6	7.47	7.23	-3.2	
	148,625 (30,167)	714 (269)	-62.3	7.62	7.45	-2.1	
	184,226 (36,845)	934 (399)	-57.3	7.70	7.66	1.2	
Average value			-54.8	7.51	7.27		
Standard deviation				0.12	0.23		
Uncertainty				1.6%	3.18%		

Tet. and Poly. tetrahedral and polyhedral, respectively; Diff. and Iter., difference and iterations and WSS, measured in Pascal.

Table 4. Summary of the results.

		With boundary layer						
	#Tet. (Poly.) cells	#Iter. Tet. (Poly.)	Difference #Iter Tet. vs. Poly. in (%)	WSS Tet.	WSS Poly.	Difference WSS Tet. vs. Poly in (%)		
Case 1	40,699 (24,206)	170 (77)	-54.7	5.48	5.45	-0.5		
	77,252 (31,548)	252 (109)	-56.8	5.93	5.82	-1.9		
	109,638 (38,564)	255 (115)	-54.9	6.20	6.00	-3.2		
	107,336 (32,012)	346 (139)	-59.8	6.02	6.04	0.33		
	124,041 (35,866)	443 (154)	-62.2	6.38	6.14	-3.8		
	160,771 (48,687)	331 (147)	-55.6	6.38	6.13	-3.9		
	202,565 (53,794)	891 (209)	-76.5	6.63	6.42	-3.2		
	228,097 (58,879)	2404 (241)	-90.0	6.68	6.49	-2.8		
	258,481 (65,707)	1804 (258)	-85.7	6.78	6.56	-3.2		
Average value			-66.6	6.62	6.40			
Standard deviation				0.12	0.14			
Uncertainty				1.79%	2.11%			
Case 2	47,311 (26,014)	256 (123)	-51.9	5.98	5.19	-13.2%		
	59,914 (21,153)	324 (180)	-44.4	6.84	6.03	-11.9%		
	75,447 (24,978)	353 (182)	-48.4	9.06	6.44	-28.9%		
	100,587 (30,435)	450 (214)	-52.4	7.11	6.53	-8.1		
	129,516 (37,221)	563 (236)	-58.1	7.19	6.80	-5.4		
	142,336 (39,833)	1705 (266)	-84.4	7.22	6.93	-4.4		
	159,797 (44,652)	684 (253)	-63.0	7.29	7.02	-3.6		
	219,922 (65,398)	1902 (320)	-83.1	7.31	7.12	-2.6		
Average value			-60.7	7.22	6.88			
Standard deviation				0.06	0.17			
Uncertainty				0.84%	2.50%			

Tet. and Poly., tetrahedral and polyhedral, respectively; Diff. and Iter., difference and iterations and WSS, measured in Pascal.

compared to the corresponding boundary layer-based tetrahedrals meshes. Even polyhedral meshes with boundary layer exhibited less than 55% NVE than tetrahedral meshes without a boundary layer.

3.2 Convergence

3.2.1 Computational convergence

Polyhedral meshes exhibited a far better convergence as tetrahedral ones as can be easily seen in Tables 3 and 4 (column 3 and 4). Polyhedral meshes needed ca. 60% (see, Tables 3 and 4, -63.7, -54.8, -66.6 and -60.7%) less iterations than the corresponding tetrahedral ones.

3.2.2 Velocity convergence

The blood flow velocity generally converged with increasing mesh size. Figure 4 illustrates the point-based measurement results regarding case 1 and case 2. For both cases, there were no significant differences between the simulated velocities of polyhedral and tetrahedral meshes.

The velocity fluctuations rapidly decreased for mesh sizes larger than 125,000 tetrahedral and 22,000 polyhedral elements in case 1 and 60,000 tetrahedral and 16,000 polyhedral elements for case 2, respectively (see, Figure 4 red bars). In the following, these mesh sizes are considered as convergence criterion and only the results of meshes larger than that are taken into account for the following velocity and WSS analysis.

Considering the data meeting the convergence criterion given above, the averaged uncertainty of the simulated velocities over all points is as follows:

- Case 1. Tetrahedral/polyhedral – 6.3/4.4%.
- Case 2. Tetrahedral/polyhedral – 1.8/1.9%.

3.2.3 WSS convergence

This section describes the WSS distribution between polyhedral and tetrahedral meshes with and without boundary layer usage. First, the results and findings of non-boundary layer meshes are presented and later in this

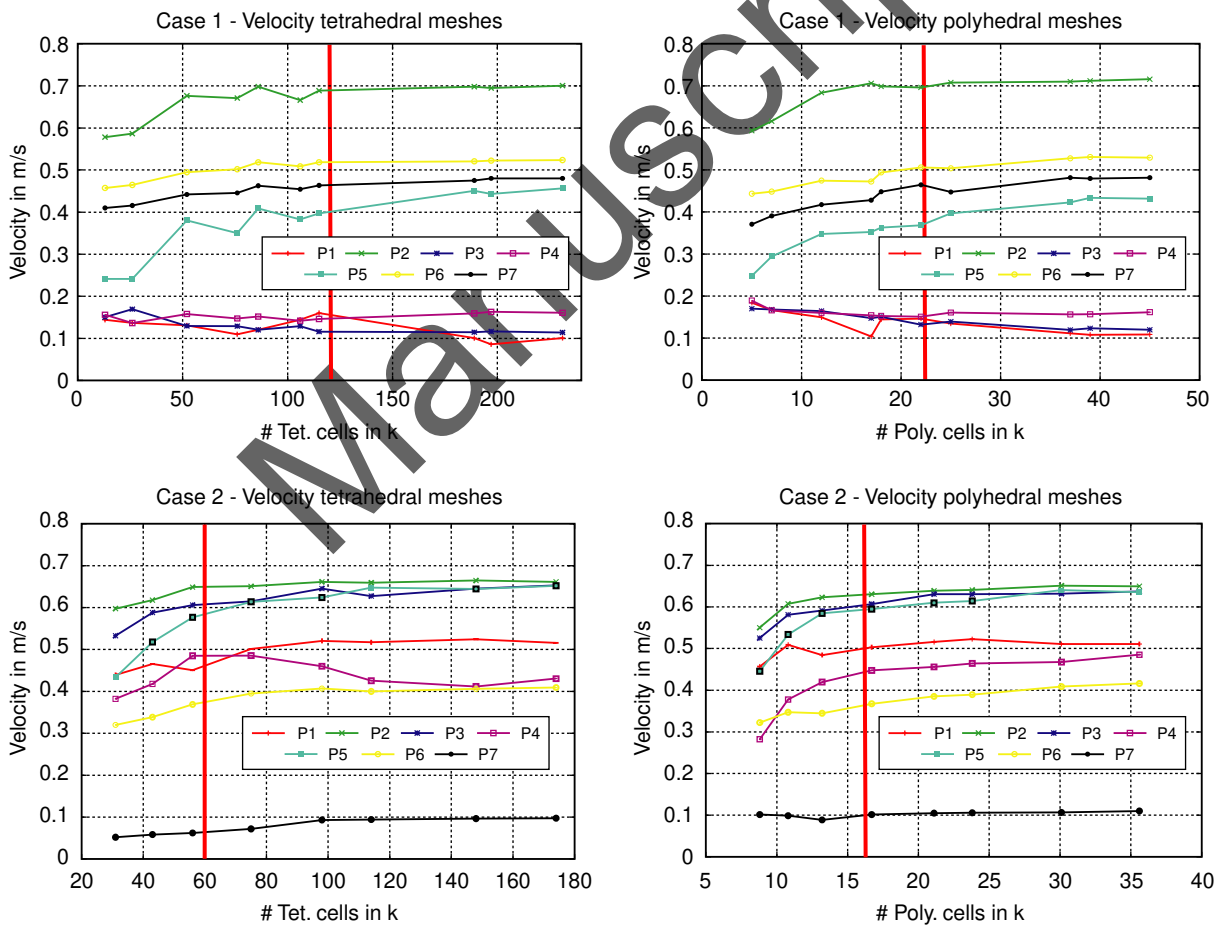


Figure 4. Velocity measurements for different mesh sizes. Top row depicts the velocity results for case 1. Bottom row illustrates the velocity values for case 2. The simulated velocities converge with increasing meshes. An increase in the mesh resolution leads to a convergence of the simulated velocity values for all point measurements. The red bar shows the border for convergence. In our study, all meshes left of the red bar are considered as non-converged velocities.

section the results of boundary layer-based meshes are shown and compared to those without a boundary layer.

The WSS results obtained without using boundary layer are presented in the left-hand side of Figures 5 and 6. The WSS pattern of polyhedral meshes appeared more homogeneous than that of the tetrahedral ones. This is illustrated by the yellow circles in Figure 5 on the left. Moreover, it turned out that polyhedral meshes were able to resolve significant WSS pattern with far less elements than the corresponding tetrahedral ones (see, Figure 5 red circles).

Table 3 (column 5/6) shows a detailed comparison regarding WSS between tetrahedral and polyhedral meshes without boundary layer. Convergence behaviour can be seen for the mesh size variations for both cases. All values highlighted in grey meet the convergence criterion and thus, being considered for the statistics, i.e. average, standard deviation (SD) and uncertainty. In case 1, the averaged WSS is 6.76 Pa, SD 0.22 Pa, (tetrahedral) compared to 6.49 Pa, SD 0.20 Pa (polyhedral). In case 2, 7.51 Pa, SD 0.12 Pa, (tetrahedral) against 7.27 Pa, SD 0.23 Pa (polyhedral).

The results for meshes with boundary layer are shown in Table 4. Again, convergence behaviour can be seen for mesh size variations with boundary layer for both cases. In

case 1, the averaged WSS is 6.62 Pa (tetrahedral) compared to 6.40 Pa (polyhedral). In case 2, 7.22 Pa (tetrahedral) against 6.88 Pa (polyhedral).

No boundary layer could be generated regarding the polyhedral mesh with the fewest NVE (see, Table 1 second row), because its approximation of the original vessel geometry is too coarse. Thus, there is no comparison with the corresponding tetrahedral mesh. The WSS pattern, obtained with a boundary layer-based mesh, is depicted in Figures 5 and 6 (right). The findings are as follows: (1) generally WSS pattern appeared smoother and better developed than those having no boundary layer and (2) however, the differences became more and more negligible with increasing mesh size, especially when comparing the highest resolved meshes as illustrated in the bottom row of Figures 5 and 6. The primary WSS pattern was also visible and recognisable without a boundary layer except for the meshes shown in the top row of Figures 5 and 6. Here, the WSS patterns considerably differ from the ones with boundary layer. But this is also due to the fact that a boundary layer-based mesh automatically exhibits more tetrahedral/polyhedral elements.

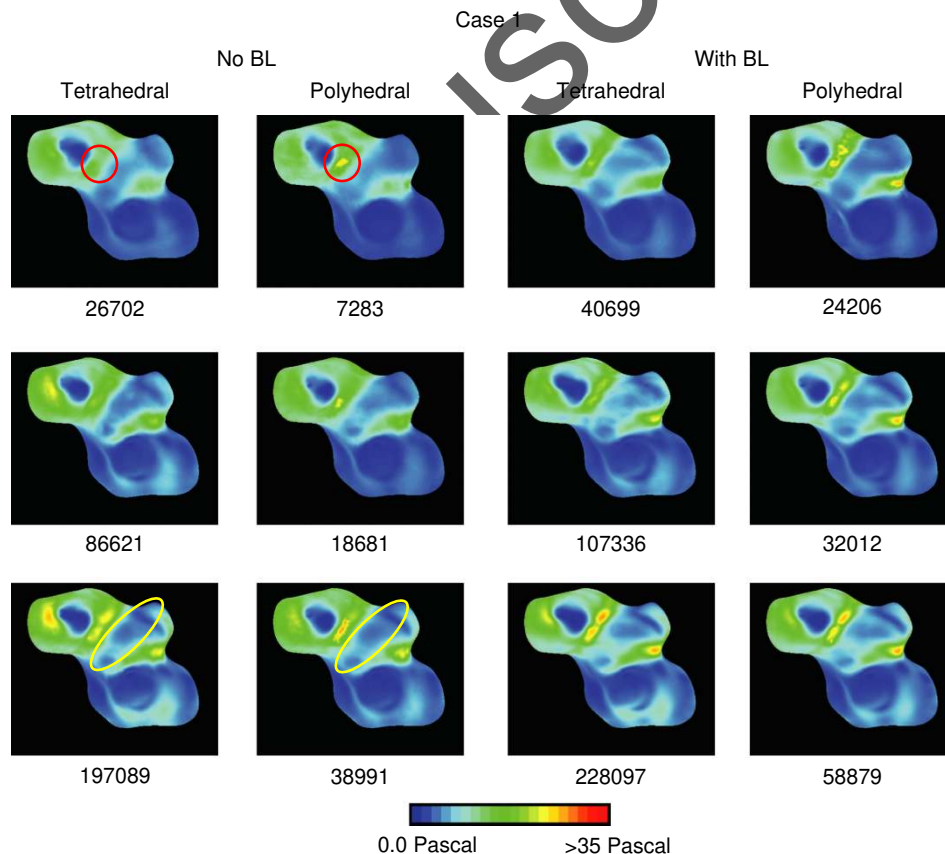


Figure 5. WSS distribution for polyhedral and tetrahedral meshes in comparison. Polyhedral meshes were also able to represent significant WSS pattern with fewer cells than tetrahedral ones as marked by the red circles. The numbers below the individual figures denote the number of cells of the mesh.

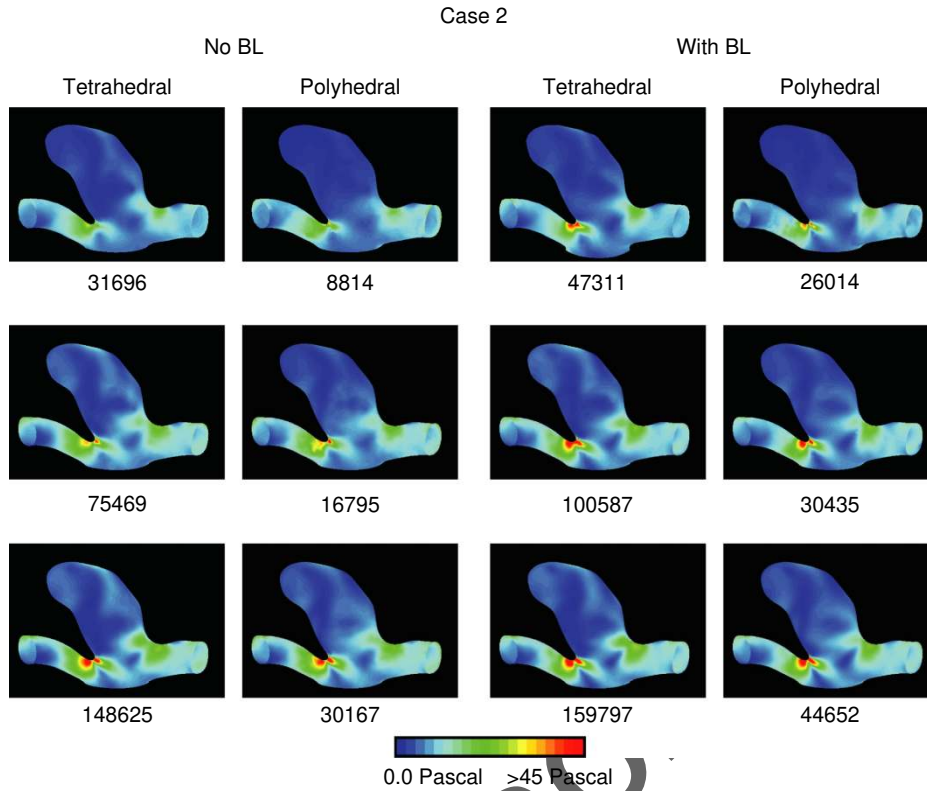


Figure 6. WSS distribution for polyhedral and tetrahedral meshes in comparison to boundary layer-based meshes. The numbers below the individual figures denote the number of cells of the mesh.

3.3 Unsteady simulation effects of varying TS size

The WSS distributions between the unsteady simulations with different TS sizes were negligible, considering the results at the moment of systole. This is shown in Figures 7 and 8. Table 5 summarises the differences in the area-weighted average WSS distribution between the different unsteady simulations averaged over the second and third cardiac cycles. The CT significantly decreased as indicated in Table 5, column 2. However, while increasing the computational TS size for the Fluent CFD solver, there are some important issues coming up: (a) the transition from one cardiac cycle to the next cardiac cycle became unstable in a sense of rapidly changing WSS distributions as illustrated in Figure 8 blue circles and (b) regarding a TS size of 0.001, the computation of each TS converged. While increasing the TS size for unsteady simulation from 0.001 to 0.005 or 0.005 to 0.01 s, the number of non-converged TS was also increasing. Consequently, the number of iterations per TS had to be increased in order to assure precise numerical simulation results. This led to increased time requirement for computation. However, the total time requirement for unsteady simulations performed with 0.005 or 0.01 s significantly decreased compared to the one with 0.001 s. The detailed time requirements for each unsteady simulation are given in Table 5.

4. Discussion

In our study, a certain threshold of the mesh resolution was required to obtain converged blood flow velocities and WSS distributions. With a resolution lower than this threshold, the velocity field and the WSS patterns fluctuated (see, Tables 3 and 4 grey areas and Figures 5 and 6). These results comply with the work of Prakash and Ethier (2001), Dompierre et al. (2002) and Lu et al. (2009) who stated that different mesh resolutions lead to different flow predictions and only mesh-independent flow solutions should be taken into account.

Once converged, WSS distributions obtained with either tetrahedral or polyhedral meshes were of similar appearance.

Table 5. Unsteady WSS simulation results – case 1 and case 2.

	CT in h (TS in s.)	Wall shear stress	
		Avg.	StDev.
Case 1	12 (0.001)	3.3832	1.4395
	4.5 (0.005)	3.2885	1.6721
Case 2	2 (0.01)	3.2893	1.6874
	7 (0.001)	5.9294	1.1007
	4 (0.005)	5.9291	1.1019
	2.5 (0.01)	5.9089	1.1019

CT and TS, computation time and time step.

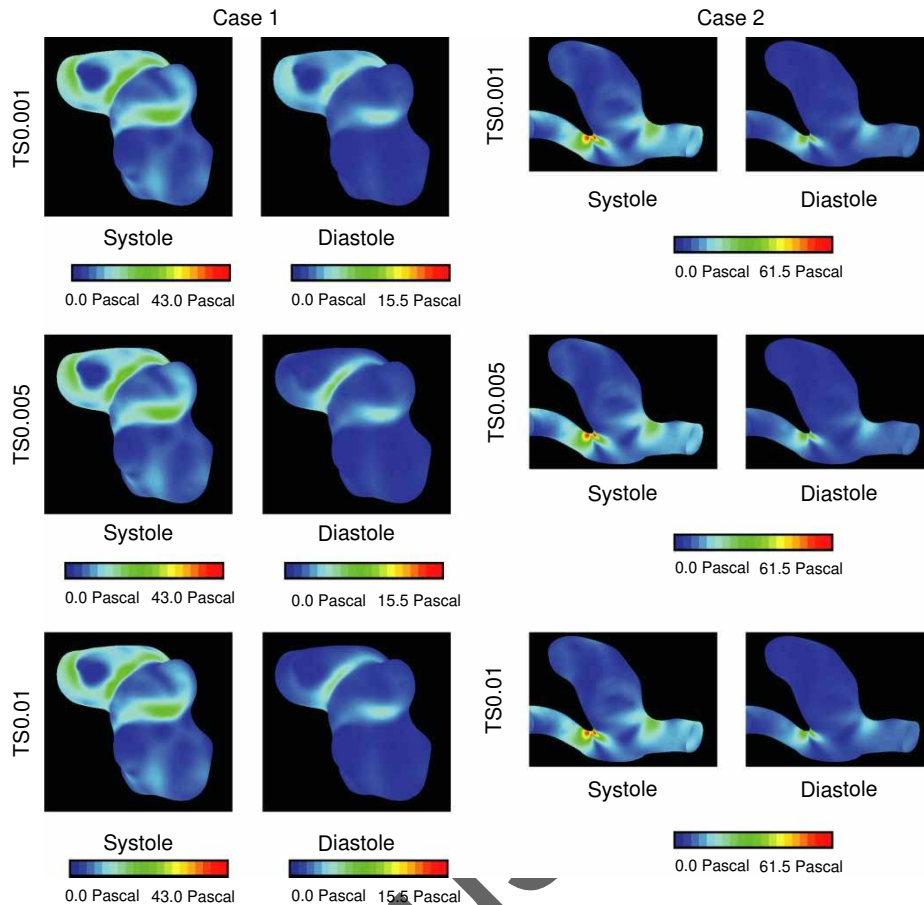


Figure 7. WSS distribution regarding unsteady simulation performed with different TS. The images show results at systole and diastole. Overall, there are no significant differences between the WSS patterns obtained from simulations with TS 0.001, 0.005 or 0.01 s.

Polyhedral meshes may, therefore, be considered as a viable alternative to tetrahedral meshes: (1) improved computational convergence as previously described by Peric (2004). This becomes very important considering the clinical applicability of CFD-based haemodynamic simulations. Future clinical CFD-based diagnostic and treatment tools have to perform fast and stable. Varying simulation parameters for convergence optimisation is not feasible during an intervention and (2) polyhedral elements resolve significant WSS pattern with far less control elements in a more homogeneous manner than tetrahedral meshes. The reason for this lies in the way the WSS magnitude is calculated which depends on two major aspects: firstly, only those cell elements are considered which actually share a face with the vessel boundary. Not all tetrahedral elements located at the vessel boundary share necessarily an entire face with the boundary – some may touch the boundary with its corner, while all polyhedral elements located at the wall share an entire face with the boundary itself. Secondly, the distances of the considered tetrahedral centres are not equal to the vessel wall leading to a more inhomogeneous WSS appearance. Polyhedral meshes should be preferred over

tetrahedral meshes in future standardised clinical simulations, since they have shown superior CFD properties in terms of better convergence and less control elements which directly lead to a shorter CT.

The usage of boundary layer leads to a more detailed appearance of WSS distributions. This occurs because the small prism elements approximate the vessel wall in denser and accurate manner.

Accurately approximating WSS on the aneurysm wall is of particular interest, as previous studies (Cebal, et al. 2005a; Jou et al. 2008) have demonstrated that aneurysms exhibiting a WSS distribution with a higher portion of lower values were more prone to expansion and perhaps rupture. Although boundary layers lead to more details in the WSS patterns, major features were already well resolved in meshes without boundary layers. The drawback of boundary layer meshes consists in their set-up resulting in an increased complexity in user interaction. Correct initiation of a boundary layer requires high smoothness and spatial resolution of the vessel surface mesh to avoid highly skewed elements at surface region exhibiting high curvature, e.g. vessel bifurcations. Extensive smoothing

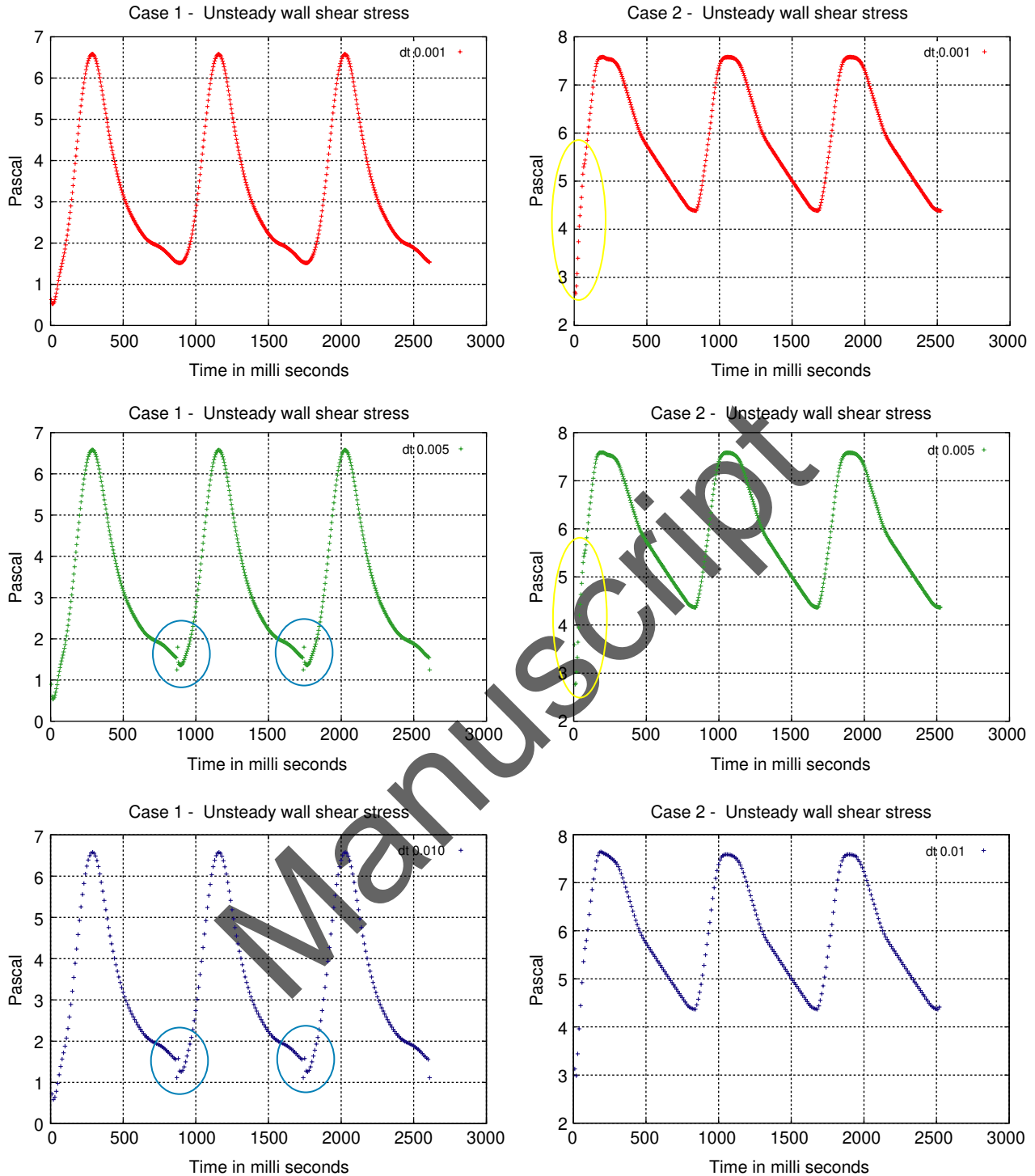


Figure 8. Area-weighted average WSS distribution values of the unsteady simulations plotted for the first three cardiac cycles. Left column shows case 1 and right column case 2. While changing the TS, the transition between cardiac cycles becomes unstable as marked by the blue circles. The yellow circle indicates the transient response at the beginning of unsteady simulations.

without close inspection by the user may lead to a deformation of the original vessel surface, i.e. shrinkness of the vessel diameter and more critical a shrinkness of the aneurysm neck potentially falsifying flow pattern and, thus, WSS distributions. Future clinical applications requiring

an automated set-up, boundary layer meshes may, therefore, be more difficult.

Another important aspect of our study is that the WSS distribution values vary even if the mesh size is considered fine enough to match the convergence criterion for our

cases (see, Section 2). Since the true WSS distribution cannot be measured *in vivo*, one has to be aware that the WSS distribution simulations have an intrinsic uncertainty. Within this study, this uncertainty for WSS values and velocities ranges between 0.84 and 6.3% comparing polyhedral vs. tetrahedral meshes with and without boundary layers. This uncertainty has to be taken into account clinically when making a quantitative statement concerning WSS, blood velocity or blood flow pattern. The key step in performing haemodynamic simulations, therefore, may be considered to generate a series of spatial varying meshes and to postulate convergence once variation of WSS falls in the range of 3–6%. If that is the case, then the mesh may be considered to be within a convergence area where mesh-independent simulation values can be computed. Given this evaluation, we propose to omit the usage of boundary layer for future clinical CFD application at least in the research phase. This will help to keep the mesh generation process simpler and easily automatable.

Unsteady simulations according to a patient-specific cardiac cycle may lead to different WSS distributions as obtained by steady simulations. However, unsteady simulations induce a much higher computational demand and thus lead to longer CT making a clinical CFD application difficult during an intervention. The CT can be minimised by either a reduction in the mesh resolution (which may lead to non-reliable results) or an increase in the computation TS governing the Fluent CFD solver for solving the Navier–Stokes equation. Our experiments have shown that an increase in the TS from 0.001 to 0.01 s does not lead to any observable changes in the WSS distribution at systole time, but a decrease in the CT by a factor of 6 (case 1) and 3 (case 2) (see, Table 3 column 2). An increase in the TS, however, has to be regarded with suspicion because there will be for sure a point once the TS is above a certain value which leads to unstable or even diverging numerical solution. Overall, the first cardiac cycle should not be used for evaluation or diagnosis, because of the transient response of the corresponding Navier–Stokes equations.

The results obtained during this study may be affected due to several limitations of the analysis. Our assumptions concerning the conducted CFD experiments differ from the *in vivo* state in terms of rigid vessel walls, Newtonian-based blood fluid and the determination of the boundary conditions. The outflows of the patient-specific models are defined as pressure outlet zero which does not have to match with the real environment. There might be natural resistances at the outflows. As with other computational studies, it is assumed that these limitations have only minor effects on the resulting flow pattern (Cebal et al. 2005b). Future work, however, has to focus on the reduction in these limitations in the sense of validation against *in vivo* measurements, perform this analysis with much more cases and repeat it for the unsteady simulation.

5. Conclusion

This study has presented the first mesh granularity and mesh independency analysis in the field of cerebral blood flow simulation of aneurysms. Here, the focus is on the influence of the CFD mesh, as aneurysms represent a complex geometry. The aim was to determine how to reduce the CT.

Our results illustrate the importance of a well-founded mesh granularity evaluation. A certain resolution is needed to obtain valid and stable WSS patterns and velocity values. However, even the CFD results of sufficient fine resolved meshes show an uncertainty of 3–6%. Polyhedral meshes are preferred for cerebral aneurysm CFD simulations due to their advantages concerning better convergence, shorter CT and high WSS accuracy. The usage of boundary layer revealed that it does not significantly change the accuracy of the WSS distributions, especially when using polyhedral cell elements. Our variations of the TS for our unsteady simulation experiments have illustrated that this leads to a reduction in time without losing significant WSS information at the systole time. This approach serves as a first key step towards a future clinical CFD application where the mesh generation process has to be automated.

The concepts and information presented in this paper are based on research and are not commercially available.

Acknowledgements

The authors would like to thank Dr Ralf Kroeger (ANSYS Germany Inc.) for his advice and simulation support. The authors gratefully acknowledge funding of the Erlangen Graduate School in Advanced Optical Technologies (SAOT) by the German National Science Foundation (DFG) in the framework of the excellence initiative.

References

- Cebal J, Castro M, Burgess J, Pergolizzi R, Sheridan M, Putman C. 2005. Characterization of cerebral aneurysms for assessing risk of rupture by using patient-specific computational hemodynamics models. *Am J Neuroradiol.* 26:2550–2559.
- Cebal J, Castro M, Appanaboyina S, Putman C, Millan D, Frangi A. 2005. Efficient pipeline for image-based patient-specific analysis of cerebral aneurysm hemodynamics: technique and sensitivity. *IEEE Trans Med Imaging.* 24(4): 457–467.
- Cebal J, Lohner R. 2005. Efficient simulation of blood flow past complex endovascular devices using an adaptive embedding technique. *IEEE Trans Med Imaging.* 24(4):468–476.
- Cooperation F. 2007. *Gambit 2.4 user's guide*. Wilmington, DE: du Pont de Nemours and Co.
- Dompierre J, Vallet MG, Bourgault Y, Fortin M, Habashi WG. 2002. Anisotropic mesh adaptation towards user-independent mesh-independent and solver-independent CFD part 3 unstructured meshes. *Int J Numer Methods Fluids.* 39:675–702.
- Garimella R, Shephard M. 2000. Boundary layer mesh generation for viscous flow simulation. *Int J Numer Methods Eng.* 49(2):193–218.

- Groden C, Laudan J, Gatchell S, Zeumer H. 2001. Three-dimensional pulsatile flow simulation before and after endovascular coil embolization of a terminal cerebral aneurysm. *J Cereb Blood Flow Metab.* 21(12):1464–1471.
- Hassan T, Ezura M, Timofeev E, Tominaga T, Saito T, Takahashi A, Takayama K, Yoshimoto T. 2004. Computational simulation of therapeutic parent artery occlusion to treat giant vertebrobasilar aneurysm. *Am J Neuroradiol.* 25(1):63–68.
- Heran N, Song J, Namba K, Smith W, Niimi Y, Berenstein A. 2006. The utility of DynaCT in neuroendovascular procedures. *Am J Neuroradiol.* 27(2):330–332.
- Hoi Y, Meng H, Woodward S, Bendok B, Hanel R, Guterman L, Hopkins L. 2004. Effects of arterial geometry on aneurysm growth: three-dimensional computational fluid dynamics study. *J Neurosurg.* 101(4):676–681.
- Jou L, Lee D, Morsi H, Mawad M. 2008. Wall shear stress on ruptured and unruptured intracranial aneurysms at the internal carotid artery. *Am J Neuroradiol.* 29(9):1761–1767.
- Karmonik C, Arat A, Benndorf G, Akpek S, Klucznik R, Mawad M, Strother C. 2004. A technique for improved quantitative characterization of intracranial aneurysms. *Am J Neuroradiol.* 25(7):1158–1161.
- Karmonik C, Klucznik R, Benndorf G. 2008. Blood flow in cerebral aneurysms: comparison of phase contrast magnetic resonance and computational fluid dynamics – preliminary experience. *Rofo.* 180(3):209–215.
- Kato T, Indo T, Yoshida E, Iwasaki Y, Sone M, Sobue G. 2002. Contrast-enhanced 2D cine phase MR angiography for measurement of basilar artery blood flow in posterior circulation ischemia. *Am J Neuroradiol.* 23:1346–1351.
- Loehner R, Cebra J. 2000. Generation of non-isotropic unstructured grids via directional enrichment. *Int J Numer Methods Eng.* 49(2):219–232.
- Lorenson WE, Cline H. 1987. Marching cubes: a high resolution 3D surface construction algorithm. *Comput Graph.* 21(4):163–169.
- Lu B, Wang W, Li J. 2009. Searching for a mesh-independent sub-grid model for CFD simulation of gas–solid riser flows. *Chem Eng Sci.* 64:3437–3447.
- Nader-Sepahi A, Casimiro M, Sen J, Kitchen N. 2004. Is aspect ratio a reliable predictor of intracranial aneurysm rupture? *Neurosurgery.* 54(6):1343–1347.
- Oaks W, Paoletti S. 2000. Polyhedral mesh generation. In: *Proceedings of the 9th International Meshing Round Table.* New Orleans Louisiana: Sandia National Laboratories p. 57–66.
- Peric M. 2004. Flow simulation using control volumes of arbitrary polyhedral shape. In: *ERCOFTAC bulletin; September, European Research Community on flow, turbulence combustion,* p. 62.
- Prakash S, Ethier CR. 2001. Requirements for mesh resolution in 3D computational hemodynamics. *J Biomech Eng.* 123:134–144.
- Raghavan M, Ma B, Harbaugh R. 2005. Quantified aneurysm shape and rupture risk. *J Neurosurg.* 102(2):355–362.
- Shojima M, Oshima M, Takagi K, Torii R, Hayakawa M, Katada K, Morita A, Kirino T. 2004. Magnitude and role of wall shear stress on cerebral aneurysm computational fluid dynamic study of 80 middle cerebral artery aneurysms. *Stroke.* 35(11):2500–2505.
- Spiegel M, Redel T, Zhang J, Struffert T, Hornegger J, Grossman R, Doerfler A, Karmonik C. 2009. Tetrahedral and polyhedral mesh evaluation for cerebral hemodynamic simulation – a comparison. In: *Multiscale Biomedical Engineering (31st Annual International Conference of the IEEE EMBS Minneapolis, IEEE Society, Minneapolis, MN, USA, September 2–6).* p. 2787–2790.
- Steinman D, Miller J, Norley C, Lownie S, Holdsworth D. 2003. Image-based computational simulation of flow dynamics in a giant intracranial aneurysm. *Am J Neuroradiol.* 24(4):559–566.
- Ujiie H, Tamano Y, Sasaki K, Hori T. 2001. Is the aspect ratio a reliable index for predicting the rupture of a saccular aneurysm? *Neurosurgery.* 48(3):495–502.
- Venugopal P, Valentino D, Schmitt H, Villablanca J, Vinuela F, Duckwiler G. 2007. Sensitivity of patient-specific numerical simulation of cerebral aneurysm hemodynamics to inflow boundary conditions. *J Neurosurg.* 106(6):1051–1060.
- Winn H, Jane J, Taylor J, Kaiser D, Britz G. 2002. Detection of asymptomatic incidental aneurysms: review of 4568 arteriograms. *J Neurosurg.* 96(1):43–49.